Stochastic dynamics simulation of surfactant self-assembly

Cite as: J. Chem. Phys. **106**, 9850 (1997); https://doi.org/10.1063/1.473873
Submitted: 14 January 1997 . Accepted: 10 March 1997 . Published Online: 31 August 1998

Friedrich K. von Gottberg, Kenneth A. Smith, and T. Alan Hatton

Stochastic dynamics simulation of surfactant self-assembly

Friedrich K. von Gottberg, Kenneth A. Smith, and T. Alan Hatton
Department of Chemical Engineering, Massachusetts Institute of Technology, Cambridge, Massachusetts 02139

(Received 14 January 1997; accepted 10 March 1997)

The self-assembly of short amphiphilic molecules of type A_2B_2 (A=hydrophilic, B=hydrophobic) is investigated using Stochastic Dynamics simulations with a scalar frictional coefficient. Equilibrium properties were calculated and explained in the context of existing thermodynamic theories. Spherical micelles are observed to form and the effect of temperature and total surfactant concentration on the structural properties are investigated. Above the critical micelle concentration, a decline in the free surfactant concentration is observed, contrary to existing theories dealing with micelle formation. The observed behavior can be explained in terms of excluded volume effects. Excellent agreement is obtained between the resulting predictions and the simulation results over the entire concentration range. © *1997 American Institute of Physics.* [S0021-9606(97)50223-6]

I. INTRODUCTION

The aggregation of surfactants in solution to form micelles and other structured microphases has long been of interest to researchers and practitioners alike, both because of important practical application areas and opportunities for these systems, and because their aggregation dynamics and thermodynamics impose challenging intellectual problems. Important properties of micellar systems include critical micelle concentrations, average size and size distributions of the micelles, and the dynamics of aggregate formation and rearrangement. Theoretical efforts to understand and predict these properties rely on both phenomenological thermodynamic analyses and atomistic simulations; each method has its own strengths and weaknesses. In this paper we explore the potential for atomistic Stochastic Dynamics simulation techniques to predict micelle equilibrium properties and point to the importance of considering excluded volume effects in the thermodynamic descriptions.

Equilibrium thermodynamic theories hinge on the ability to calculate the chemical potential of free and associated surfactant molecules.[1–6] Thus, various shapes of the aggregate structure are assumed and the free energies for these structures calculated. That structure having the lowest energy is selected as the equilibrium structure for the conditions of interest. These existing theories have been somewhat successful in predicting micelle formation, size distributions, and in identifying phase boundaries. They are unable to probe the dynamics of micellar systems, however, or to identify transition states or pathways by which these systems evolve. Indeed, the requirement for the *a priori* specification of the micelle structure precludes the identification of unexpected novel aggregate structures, a limitation that can only be overcome through atomistic-type simulations.

Extensive Monte Carlo simulations of amphiphile-water-oil systems have provided phase diagrams[7,8] and identified the structure and occurrence of micelles.[9] Symmetric diblock[10] and triblock[11] copolymer micelles have also been investigated but, due to the length of the amphiphile chains considered, very long simulations are required to sample equilibrium properties. Desplat and Care[12] recently modeled a short surfactant chain (AB_3) and used the resulting equilibrium micelle size distribution to extract the excess chemical potential ($\mu_s^o - \mu_1^o$) which was then compared to existing analytical expressions.[13] These simulations have been limited to lattices which may influence the structure of the aggregates formed. In addition, this approach cannot easily be extended to branched amphiphiles and the observed dynamics are determined by the reptation techniques employed.

Molecular Dynamics simulations of surfactant aggregates fall into two categories. Firstly, the surfactant models used may involve complicated all atom potentials in an attempt to represent real surfactants and solvents. Since this approach is computationally intensive, the micelle structures have to be preassembled (i.e., the structure must be selected *a priori*) and only a single aggregate may be simulated for short periods (typically less than 0.1 ns). Examples of this work include reverse micelles,[14] n-decyltrimethylammonium chloride micelles in water,[15] and sodium octanoate micelles.[16] This method is not suitable for probing the dynamics of self-assembly. In addition the final structure relies heavily on the choice of initial structure. The second approach uses simplified surfactants (having only the essential characteristics of amphiphiles) but allows the surfactants to self-assemble into the structures they prefer.[17,18] At best, qualitative behavior may be obtained from such model systems. Large scale parallel Molecular Dynamics simulations have been employed[19] and used to investigate the effect of different surfactant structures[20,21] and probe the mechanism of oil solubilization.[22] Equilibrium properties are still beyond the scope of these techniques even with current computational capabilities. The inability to sample the configurational phase space using conventional techniques is exemplified by recent MD simulations probing the effect of chain length[23] and the presence of solutes on micelle formation.[24]

In this work a coarse-grained bead-rod model representation of the surfactant molecule is employed. In an effort to reduce the problem complexity, solvent effects are incorpo-

 0021-9606/97/106(23)/9850/8/$10.00

rated through a stochastic noise term in the equation of motion. This is accomplished by performing Stochastic Dynamics simulations, a simplification which enables us to perform the longer simulations required to monitor the self-assembly process and to extract equilibrium data for model amphiphile systems.

II. METHODOLOGY

The number of degrees of freedom involved in simulating a self-assembling surfactant solution can be substantially reduced by omitting the solvent molecules. This can be justified on the basis that the timescale associated with their motion is much shorter than that of the surfactant molecule itself. The effect of the solvent is retained as faithfully as possible, however, by incorporating random forces to account for uncorrelated solvent contributions,[25,26] and by introducing a modified force field (potential of mean force[27,28]) to account for the influence of the solvent molecules on the solute (in our case the surfactant molecule). This approach is generally referred to as Stochastic Dynamics (SD). Prior applications of SD include simulations of n-alkanes and polymers,[26,29,30] peptides,[31] a lipid chain in a membrane bilayer,[32] solvent effects on dendrimer conformation,[33] and confined polymer melts.[34]

A. Simulation details

The surfactant molecule is treated as consisting of a series of particles linked together via rigid bonds. The equation of motion for each particle i is[26]

$$m_i\dot{\mathbf{v}}_i(t) = -m_i\xi_i\mathbf{v}_i(t) + \mathbf{F}_i(\{\mathbf{x}_i(t)\}) + \mathbf{R}_i(t), \tag{1}$$

where m_i is the mass of particle i and $\mathbf{x}_i$, $\mathbf{v}_i$, $\mathbf{F}_i$, and ξ_i represent the position, velocity, force, and frictional (damping) coefficient acting on particle i, respectively. Equation (1) represents the simplest form of SD in which the time and spatial correlations in the frictional coefficient are neglected. It is commonly referred to as Brownian Dynamics (BD).

The stochastic force $\mathbf{R}_i$ is assumed to be stationary, Markovian and Gaussian with zero mean and to have no correlation with prior velocities nor with the systematic force. These requirements dictate that $\mathbf{R}_i$ must satisfy the conditions

$$\langle \mathbf{R}_i(t) \rangle = 0, \tag{2}$$

$$\langle R_{i\alpha}(t) R_{i\beta}(t') \rangle = 2k_B T \xi_i m_i \delta_{i,j} \delta_{\alpha,\beta} \delta(t-t'). \tag{3}$$

The indices α, β denote the Cartesian coordinate directions (x,y,z) while i, j denote particle labels. The stochastic noise term acts as a heat bath to compensate for the energy sink due to viscous drag. The stationary solution is the Boltzmann distribution and hence these simulations produce canonical time averages (NVT ensemble). The dynamical properties are changed depending on their relaxation rate by the presence of the heat bath. To generate the correct gas phase MD dynamical behavior, ξ^{-1} must be larger than the relaxation time of the property of interest. On this timescale, however, the canonical ensemble is no longer simulated. On longer timescales, the dynamics are purely diffusive (Rouse-like dynamics). Equilibrium results are independent of the choice of the friction coefficient ξ and correspond to a gas phase constant temperature MD simulation with the same force field ($\mathbf{F}_i(\{\mathbf{x}_i(t)\})$). The utility of this approach is that the effect of the solvent on the dynamics should be realistic at long times.

A third order SD integration algorithm was implemented based on the work of Gunsteren and Berendsen.[35,36] An important feature of this algorithm is that the integration timestep (Δt) is not restricted by ξ, since the stochastic force has been integrated over the interval Δt. Hence, the size of the timestep is determined only by the rate of change in the systematic force i.e. on the interatomic potential.

B. Model system

The surfactant molecules are represented by a coarse grained bead-rod model. Physically each bead may be thought of as being equivalent to a Kuhn length (order 10 methylene groups) on a polymer chain.[37] Bond lengths were constrained iteratively using the SHAKE algorithm[38,39] with $tol = 10^{-5}$. Bond angle constraints were not included, so the simulations represent flexible chains. Unshifted Lennard-Jones (LJ) interactions were employed between the beads, the nature of which could be varied by changing the cut-off distance r_c,

$$\phi(r) = \begin{cases} 4\epsilon\left[\left(\dfrac{\sigma}{r}\right)^{12} - \left(\dfrac{\sigma}{r}\right)^{6}\right] & r \leqslant r_c \\ 0 & r > r_c \end{cases}, \tag{4}$$

where r is the separation distance and ϵ and σ are the well depth and size parameter in the LJ potential.

Short diblock amphiphiles of type A_2B_2, where A and B are the hydrophilic and hydrophobic blocks respectively, were simulated. The $B-B$ interactions were LJ attractive with a conventional cut-off distance of $r_c = 2.5\sigma$ while $A-B$ and $A-A$ interactions were purely repulsive ($r_c = 2^{1/6}\sigma$). All beads were taken to have equal mass (m) and frictional coefficient (ξ). Bond lengths were constrained to $2^{1/6}\sigma$.

Initially the surfactant chains were arranged on a fcc lattice. The surfactant concentration is given as a bead number density ($[S] = N_s N_b / V$, N_s is the number of surfactant molecules, N_b is the number of beads per surfactant molecule, and V is the simulation volume), which is directly proportional to volume fraction. Temperature is expressed in reduced units ($T_r = k_B T/\epsilon$) and a reduced timestep ($t_r = t/\sigma\sqrt{(m/\epsilon)}$) of length $\Delta t_r = 0.005$ was used. The reduced frictional coefficient is given by $\xi_r = \xi\sigma\sqrt{(m/\epsilon)}$. Most simulations were performed at two system sizes (108 and 256 surfactants). No effect of system size was noted. At high number density ($[S] \geqslant 0.10$) 864 surfactants were used in the simulations. The simulations were run on a HP 735/125 MHz workstation which took $2.\times 10^{-4}$ cpu seconds/timestep/molecule at $[S] = 0.12$. Typically 5-15 million timesteps were performed per simulation depending on system size.

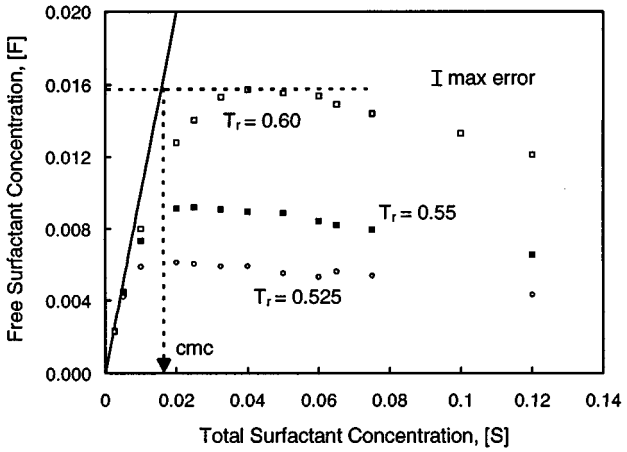

FIG. 1. Variation of free surfactant concentration ($[F]$) with total surfactant concentration ($[S]$) indicating the onset of micellization and the definition of cmc.

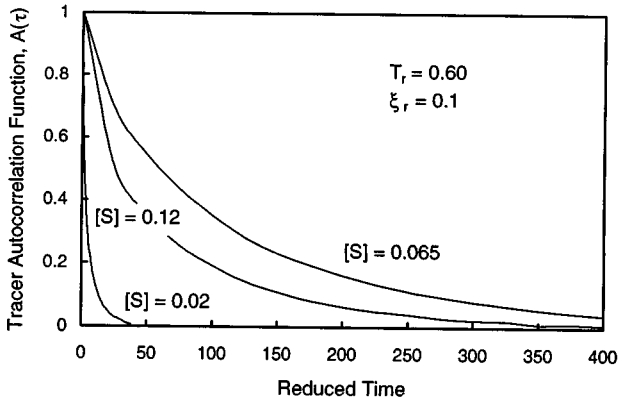

FIG. 2. Tracer autocorrelation function ($A(\tau)$) for different total surfactant concentrations ($[S]$) at $T_r=0.60, \xi_r=0.1$.

Surfactant chains were designated as belonging to an aggregate if any tail beads (B beads) of the surfactants were within a certain distance of each other ($r_{\text{clust}}=1.5\sigma$).[19]

III. SIMULATION RESULTS AND DISCUSSION

Each simulation trajectory was divided into two sections once equilibrium had been established. Equilibrium properties with error bounds were then calculated for these two sections by further subdivision into 5 parts. This procedure enabled us to determine if any drift in calculated values was evident from the first half of the simulation to the second half. Typically, the drift was well within the error bounds of the calculated values. For clarity, only the maximum error bar ($\pm$ standard deviation) is shown in the figures.

A. Equilibrium properties

The onset of micellization is traditionally depicted by plotting the free (non-associated) surfactant concentration ($[F]$) as a function of the total surfactant concentration ($[S]$). Above a certain total surfactant concentration, called the critical micelle concentration (cmc), $[F]$ levels off. Figure 1 shows this behavior at three temperatures. The cmc increases with increasing temperature as would be expected for a system with an enthalpic driving force for micellization. At higher concentrations, a decline in free surfactant concentration is observed. Most existing theories[1,6,13,40] suggest that the free surfactant concentration should remain constant or increase slightly above the cmc. An explanation for this deviation from ideal behavior is provided in the next section.

By labelling a chain in an aggregate and then following the size of the aggregate in which the chain resides, one can observe how the chain samples aggregates of different sizes. This chain is referred to as a tracer chain. A tracer autocorrelation function[41] was used to estimate the correlation times within the system and hence to obtain a qualitative idea of the simulation times required to sample the equilibrium state of the system, where

$$A(\tau)=\frac{\langle N(t+\tau)N(t)\rangle-\langle N(t)\rangle^2}{\langle N^2(t)\rangle-\langle N(t)\rangle^2}, \tag{5}$$

and $N(t)$ is the aggregate size in which the tracer chain resides at time t. The angular brackets indicate an ensemble average over all molecules taken successively as tracer chains in addition to averaging over multiple time origins t. For $\tau=0$, $A(\tau)=1$ (perfectly correlated) while as $N(t+\tau)$ becomes uncorrelated with $N(t)$, $A(\tau)\to 0$. The tracer autocorrelation function provides an indication of how long it takes a tracer chain to sample all aggregate sizes. A correlation time (τ_c) was defined as the time required for $A(\tau)$ to reach a value of e^{-1}. At $[S]=0.02$, before micelles form, $\tau_c=5$ (Fig. 2, $\xi_r=0.1$). Above the cmc, at $[S]=0.065$ the correlation time is of the order $\tau_c=125$, decreasing as the micelle concentration increases ($\tau_c=80$, $[S]=0.12$). This decrease in τ_c is quantitatively consistent with the decrease in diffusional length between micelles due to the higher concentration. These results were checked and found to be independent of system size. They are, however, a function of ξ_r since this determines the diffusive timescale for the free surfactants. Typically, simulations were run from 300-600 times the tracer correlation time.

An important consideration when simulating micelle formation is that the system should not undergo macroscopic phase separation (e.g. into water and surfactant rich phases respectively). In our work, the invariance of the micelle size distribution as a function of time provided an indication that we were dealing with a homogeneous phase. Furthermore, Larson[7,9] and Mackie *et al.*[8] have performed Monte Carlo lattice simulation of A_2B_2 surfactants at $\chi=zN_b\Delta w/kT=16$ (z=lattice coordination number=26, N_b=surfactant chain length=4, $\Delta w=\epsilon_{AB}-\frac{1}{2}(\epsilon_{BB}+\epsilon_{AA})$) and determined the phase behavior. The ternary phase behavior (oil-B, water-A, surfactant-A_2B_2) at $\chi=16$ showed two and three phase regions. In a system without an oil phase, however, no phase boundary is evident.[8] At $\chi=16$, no micelle formation was observed by Larson.[9] Direct comparison with our work

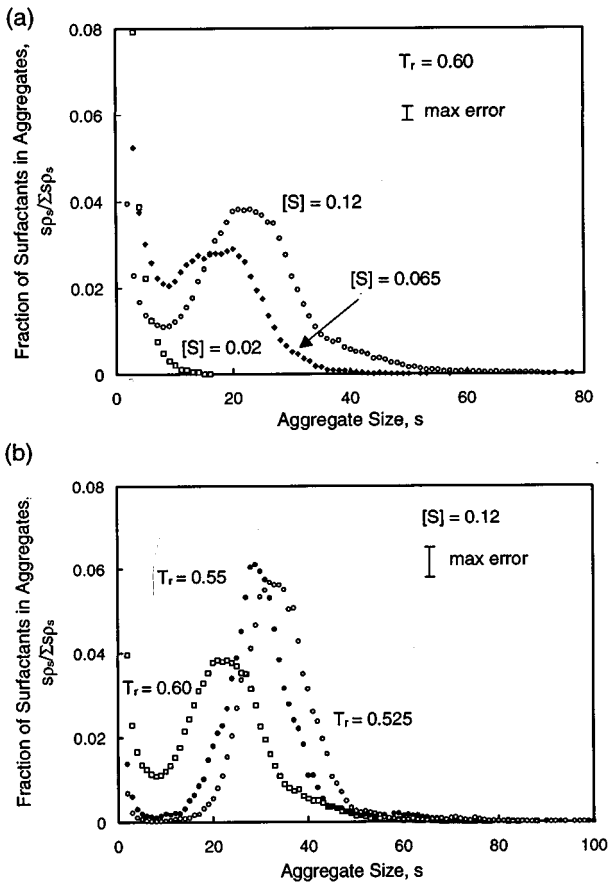

FIG. 3. Effect of (a) $[S]$ at $T_r=0.60$ and (b) T_r at $[S]=0.12$ on micelle size distribution. ρ_s is the number density of aggregates with aggregation number s.

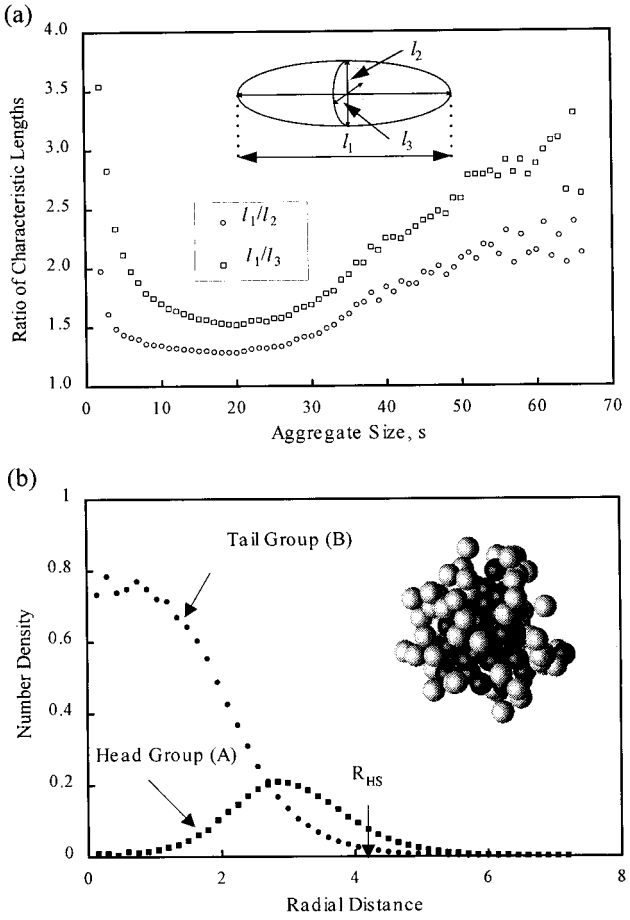

FIG. 4. (a) Ratio of characteristic lengths as a function of aggregate size ($T_r=0.60$,$[S]=0.12$). (b) Spherically averaged radial distribution function through micelle with aggregation number s=30. Inset : Snapshot of micelle (s=30), dark beads represent tail groups.

is difficult since we are dealing with an off-lattice simulation and continuous interaction potentials. However, selecting a coordination number of 11 (which corresponds to the first coordination shell), and converting our reduced temperature to that of Larson (in their notation $\epsilon_{ow}=\epsilon_{ww}=0$ and $\epsilon_{00}=-1$), we get $\chi\approx 35$. Our temperature is therefore considerably lower (factor of 2) than that used by Larson and hence it is not surprising that micelles do in fact form.

Figure 3(a) shows the simulated size distribution at three concentrations for a reduced temperature of $T_r=0.60$. For $[S]=0.02$ no micelles form because this concentration is below the cmc. As the concentration increases, a well developed maximum appears associated with the formation of spherical micelles. A shoulder in the size distribution at $s\approx 40$ is visible for $[S]=0.12$ which is associated with a transition to rod-like micelles at higher concentrations (this is confirmed by a transition in the observed hard sphere radius of the system, which is discussed later). Similarly Fig. 3(b) shows the effect of the reduced temperature on the micelle size distribution for $[S]=0.12$. At lower temperatures the shoulder in the distribution has been reduced as spherical micelles are more strongly favored.

An approximate idea of the shape of the aggregates can be obtained from the principal moments of inertia for each aggregate. This is achieved by calculating the ordered set (max→min) of eigenvalues $(\lambda_1,\lambda_2,\lambda_3)$ of the moment of inertia matrix. A characteristic length may be defined as $l_i=\sqrt{\lambda_i}$ for $i=1,2,3$. A measure of the aggregate asphericity may then be obtained by monitoring $\langle l_1\rangle/\langle l_2\rangle$ and $\langle l_1\rangle/\langle l_3\rangle$ as functions of aggregate size as shown in Fig. 4(a). The micelles with aggregation numbers 10-35 appear to be almost spherical with aspect ratios of between 1.2-1.8. The aspect ratios for essentially spherical micelles are greater than unity because this technique of characterizing the micelle shape will always select the largest and shortest dimensions at a particular instant in time. Fluctuations in micelle shape, whether due to thermal motion or monomer insertion, are therefore accentuated and will not be averaged out. For low values of s, say $10<s<20$, cylindrical micelles are virtually forbidden on geometric grounds; so this phenomenon must be entirely responsible for asphericity in this range. Micelles with aggregation numbers outside the 10-35 range are highly aspherical, but are limited to aspect ratios of less than 4. At large aggregation numbers, poor sampling is evident since these micelles occur very infrequently.

Figure 4(b) shows the spherically averaged radial distribution function through a micelle with aggregation number

of 30. The micelle is found to be composed of a dense hydrophobic core (with number density ≈ 0.78) surrounded by a less well defined corona of the hydrophilic headgroups. The corona region is considerably hydrated ($\approx 55\%$ solvent). Had the micelle been rod-like, long tails in the head and tail group distributions would have been expected. In this work, such tails were found to occur only for aggregation numbers >40.

B. Effect of excluded volume on free surfactant concentration

At surfactant concentrations well above the cmc there is a drop in [F] (Fig. 1), which has also been observed in simulations by Adriani *et al.*[42] and Desplat and Care.[12] Experimental evidence also exists for this decrease[43,44] which is not predicted by traditional theories[1,6,13,40] for micelle formation. As noted by Adriani *et al.*,[42] Leibler *et al.*'s theory[45] can, however, predict a decrease in $[F]$ since they base the entropy of mixing of the free surfactant molecules on the solvent volume and not on the solution volume. Leibler's theory suggests that excluded volume effects introduce non-ideal behavior at high $[S]$ and that the accessible volume is considerably reduced from the total solution volume. Desplat and Care[12] introduced an activity coefficient (γ) to account for these non-idealities, postulating $\ln(\gamma)$ to be proportional to the total amphiphile concentration, but independent of the aggregate size or shape. An alternative approach is employed in this work in which the activity coefficient is calculated on the basis of a virial expansion.[46] The advantage of this approach is that the physical significance of the activity coefficient and its dependence on aggregate size becomes clear. By equating the chemical potential of a free surfactant molecule to that of a surfactant molecule in an aggregate of size s, accounting for the translation entropy using an ideal gas model, and incorporating deviations from the ideal gas model into an activity coefficient, one can obtain for the aggregate size distribution[47,48]

$$\rho_s = \rho_1^s \frac{\gamma_1^s}{\gamma_s} \exp\left(\frac{-s(\mu_s^o - \mu_1^o)}{kT}\right), \tag{6}$$

where ρ_s and γ_s are the number density and activity coefficient of an aggregate of size s respectively, and μ_s^o is the chemical potential of a single surfactant molecule in an aggregate of size s in the dilute reference state (T, P, $\Sigma_s \rho_s \to 0$). If only the excluded volume effects between micelles are considered and if only the second virial term is retained in a virial expansion, the activity coefficient can be shown to be[46,47]

$$\ln(\gamma_s) = -\sum_r \beta_1(s,r)\rho_r, \tag{7}$$

where $-\beta_1(s,r)$ is the volume excluded to aggregates of size s due to the presence of aggregates of size r and is related to an interaction potential ($u_{s,r}$) between aggregates of size s and r by

$$-\beta_1(s,r) = -\frac{1}{V}\int \left[\exp\left(-\frac{u_{s,r}}{kT}\right) - 1\right] d\mathbf{q}_r d\mathbf{q}_s, \tag{8}$$

where $\mathbf{q}_r$ and $\mathbf{q}_s$ are the coordinate vectors of aggregate r and s respectively.

As $\Sigma_r \rho_r \to 0$, $\gamma_s \to 1$, and the non-interacting result is recovered. This approach is entirely analogous to that used in incorporating excluded volume effects to describe real fluids, which yields the very successful van der Waals equation of state.

It is our goal to calculate the activity coefficients from simulation data using Eq. (7) at a particular concentration ($[S]=0.12$) and then to extract the reference state chemical potentials (μ_s^0) from the simulated size distribution using Eq. (6). The μ_s^0 are independent of concentration, and hence we should be in a position to predict both the size distributions and $[F]$ for any $[S]$ using the data calculated at $[S]=0.12$. The ability to predict properties at other concentrations would strongly suggest that excluded volume effects are in fact responsible for the observed deviations. Desplat and Care,[12] in contrast, used simulation information over the entire concentration range to extract the activity coefficient. In order to calculate the activity coefficient by using Eq. (7), the size distribution (ρ_s) and structure of aggregates is required. The size distribution for $[S]=0.12$, $T_r=0.60$ is shown in Fig. 3(a).

If it is assumed that the aggregates are spherical in shape, a hard sphere radius may be defined as the radius that includes 90% of all beads within an aggregate. This information may be obtained from the radial distribution profile [Fig. 4(b)]. For spherical micelles, $R_s \propto s^{1/3}$, where the proportionality constant may be directly obtained from simulation data. Figure 5(a) shows a plot of the the effective hard sphere radius versus $s^{1/3}$, where the transition from spherical to cylindrical micelles manifests itself as a sharp change in the slope of the curve. For aggregation numbers less than 35, the aggregates are almost spherical as discussed earlier. Above 35, the aggregates are cylindrical in shape. These cylindrical micelles are ill defined and comprise two spherical micelles which are in close contact. Therefore the slope in Fig. 5(a) more than doubles as one enters the cylindrical region. Figure 5(b) shows the bead distribution projected onto the major principal axis for an aggregate of size 41. Only beads within a distance of 0.75σ from the major principal axis are included in this distribution. Close to the center of the aggregate, a marked decrease in the hydrophobic chain density is observed at the point of contact between the two aggregates. Also evident is the presence of A beads near the center of the aggregate. Sampling statistics are poor since these aggregates occur infrequently. By requiring 90% of the beads to be within R_{HS}, the aspherical nature of the aggregate is emphasized. Hence an alternative definition of an effective hard sphere radius was employed based on the radius at which the total spherically averaged bead number density$=0.12$ (equal to [S]). The latter approach has the advantage that no transition in R_{HS} is observed [Fig. 5(a)] since the bead contribution is weighted by r^{-2}, where r is distance from the center of mass. The volume occupied by a surfactant is slightly

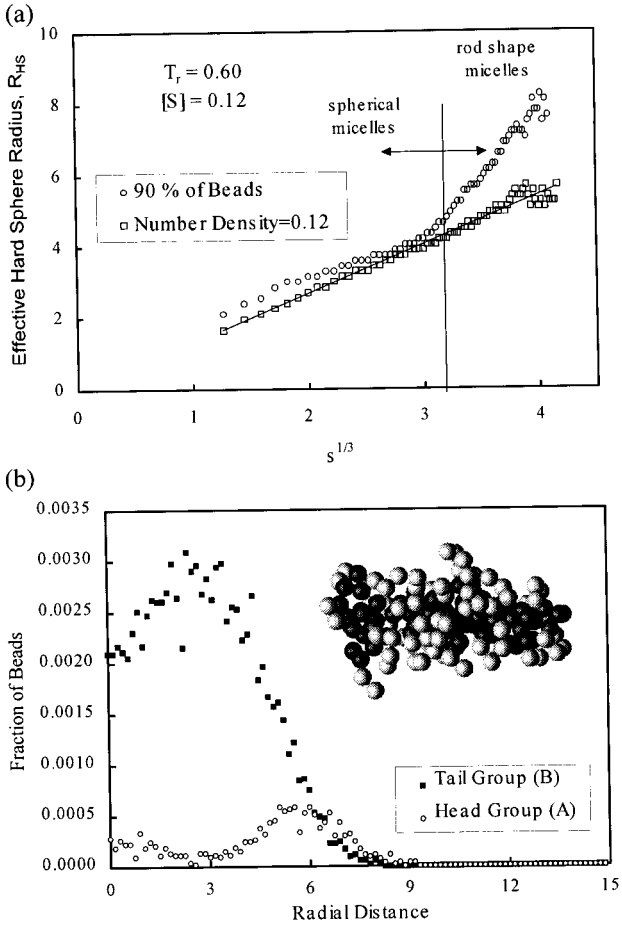

FIG. 5. (a) Variation of R_{HS} with aggregation number ($T_r = 0.60, [S] = 0.12$). (b) Bead distribution projected onto the major principal axis for micelle with s=41. Inset: Snapshot of micelle (s=41) showing rather loose and elongated structure.

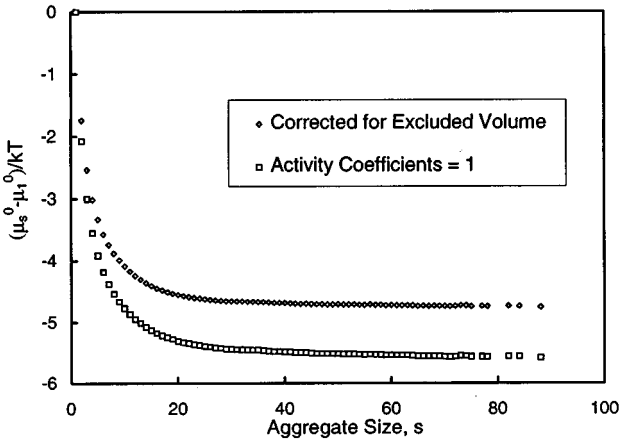

FIG. 6. Difference in chemical potential per surfactant molecule in a micelle of size s and a free surfactant molecule, $(\mu_s^o - \mu_1^o)/kT$, at $T_r = 0.60, [S] = 0.12$.

larger for higher aggregation numbers, as reflected in the negative intercept of 0.1 in Fig. 5(a).

To simplify the analysis, the excluded volume of the cylindrical micelles is assumed to be equivalent to a hypothetical spherical micelle of the same aggregation number, obtained by extrapolating the results for the spherical micelles to higher aggregation numbers. The excluded volume of the cylindrical micelles is thus underestimated, but as they are few in number their contribution is small, and the error associated with this assumption is not significant. Similarly the free surfactant effective hard sphere radius was calculated by extrapolation to an aggregation number of 1.

For interaction between hard spheres, the excluded volume may be obtained from Eq. (8) as

$$-\beta_1(s,r) = \frac{4\pi}{3}(R_r + R_s)^3. \tag{9}$$

R_r and R_s are the hard sphere radii of aggregates of size r and s respectively, as depicted in Fig. 5(a). By using the size distribution (ρ_s) and hard sphere radius of micelles (R_s) generated from the computer simulations we calculated the activity coefficients (γ_s) using Eq. (7). Using Eq. (6), one can extract from the simulated size distribution the difference in chemical potential per molecule $(\mu_s^0 - \mu_1^o)/kT$ as reported in Fig. 6. The chemical potential difference is, as noted by Desplat and Care,[12] a monotonically decreasing function in s, although in our work the decline is less pronounced. Direct comparison is difficult since they employ a amphiphile of form AB_3 and include attractive head-solvent interactions. It should be noted that incorporation of excluded volume effects serves to lower the absolute magnitude of the extracted reference state chemical potential difference, from which it follows that the observed excluded volume effects favor the formation of larger aggregates. The ratio of the volume excluded to a free monomer due to the presence of 30 free surfactants to that excluded to a monomer by an aggregate of size 30 is approximately

$$\left.\frac{30(1+1)^3}{(1+s^{+\frac{1}{3}})^3}\right|_{s=30} \sim 3.5.$$

Larger aggregates are therefore favored since they serve to reduce the total excluded volume, but this is at the expense of considerable translational entropy.

The excluded volume contribution to the chemical potential difference is

$$\ln(\gamma_1) - \frac{\ln(\gamma_s)}{s}.$$

For large s, the excluded volume contribution is predominantly determined by the first term. However, for intermediate values of s, which correspond to the observed micelle size, the contribution from the γ_s term is significant. It is therefore imperative that the size dependency of γ_s is taken into account correctly.

To quantify the size of the virial term, it is instructive to compare the contributions of the excluded volume effect and of the translational entropy to the Gibbs free energy of an aggregate of size s. The ratio is simply

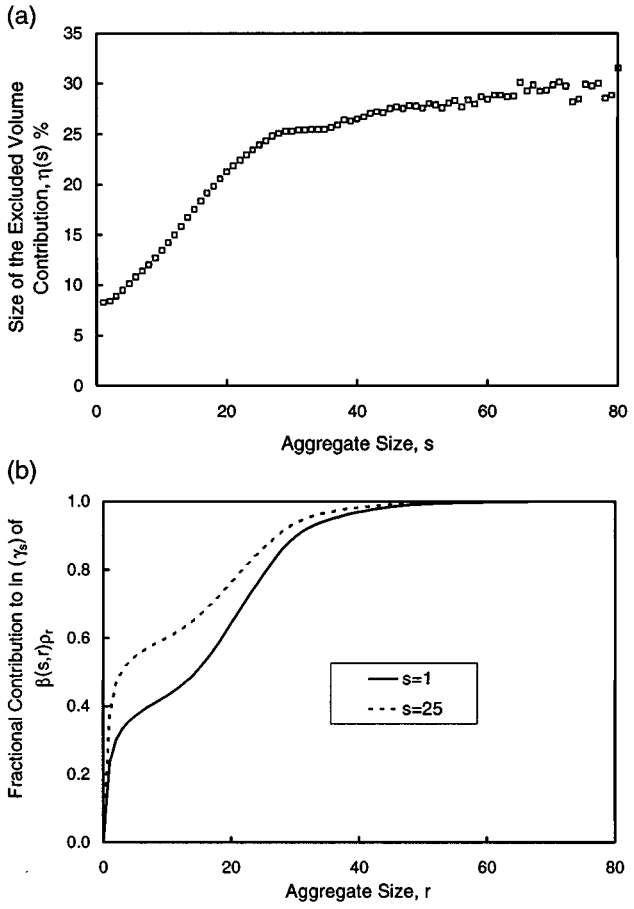

FIG. 7. (a) Contribution of virial term to translational component of Gibbs free energy as a function of aggregate size. (b) Fractional contribution of aggregates of size r to the total excluded volume for $s=1$ and $s=25$ as defined by Eq. (11).

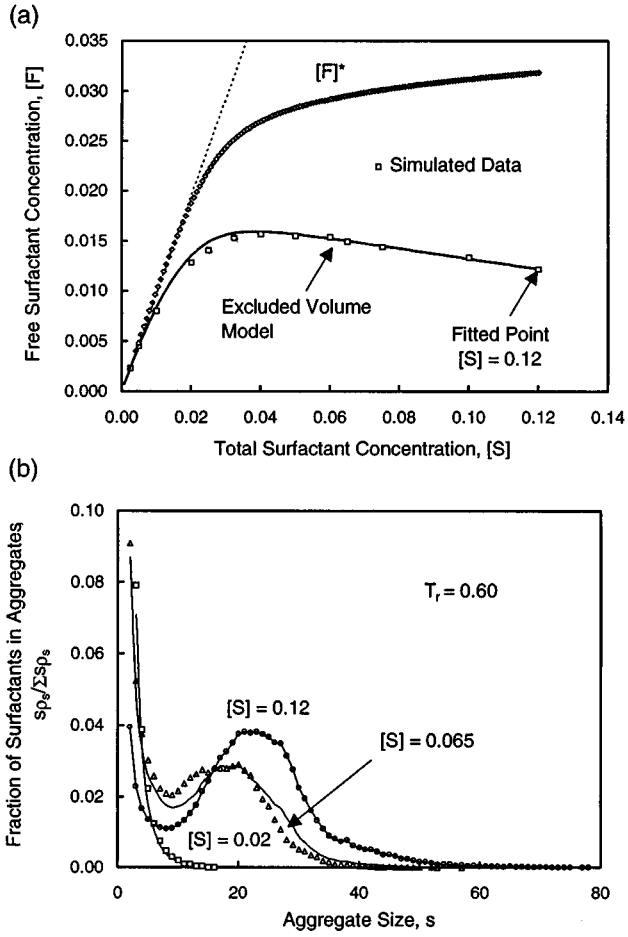

FIG. 8. Comparison of theoretical predictions to simulation data (a) Free surfactant concentration ([F]) as a function of total surfactant concentration ([S]). (b) Size distributions at different total surfactant concentration ([S]).

$$\eta(s)=\left|\frac{\ln(\gamma_s)}{\ln(\rho_s)}\right|\times 100\% \tag{10}$$

and is shown in Fig. 7(a). For small aggregate sizes, the excluded volume term contributes less than 10%, increasing to around 30% for $s>60$. Higher order virial terms are expected to play a role for large aggregates. However, since these aggregates occur so infrequently this correction was not incorporated.

Figure 7(b) shows the fractional contribution of the excluded volume terms to $\ln(\gamma_s)$ for $s=1$ and $s=25$. The fractional contribution, $\mathscr{F}(s,r)$, is defined as

$$\mathscr{F}(s,r)=\frac{\beta_1(s,r)\rho_r}{\Sigma_i\beta_1(s,i)\rho_i}. \tag{11}$$

The free surfactants (r=1), contribute significantly to the activity coefficients. For s=1, $\mathscr{F}(1,1)\approx 0.25$ due to the high number density of free surfactants. As evident from Fig. 7(b), the free surfactant contribution becomes more significant at larger s ($\mathscr{F}(25,1)\approx 0.4$). Pre-micelles (aggregation numbers 5-15) contribute significantly less than the free surfactants despite their large volumes owing to their low number density as indicated by the slight shoulder in Fig. 7(b). Aggregates with $r>40$ contribute less than 5% towards $\ln(\gamma_s)$ and thus the error introduced by assuming that the larger aggregates are spherical should be minimal.

Since values of $(\mu_s^0-\mu_1^0)/kT$ are based on an infinitely dilute reference state, they are applicable at other concentrations. We are thus in a position to predict both the size distributions and [F] for any [S] using the data calculated at [S]=0.12. This involves solving the set of equations [Eq. (6)] for ρ_r subject to the requirement that $\Sigma_r r\rho_r=[S]/N_b$. Shown in Fig. 8(a) is a comparison of the simulated data to those predicted using Eq. (6), where the agreement is seen to be excellent over the entire concentration range. Excluded volume effects thus appear to be responsible for the reduction in $[F]$ with increasing total surfactant concentration. The activity coefficient may be included in the definition of a new concentration variable $[F]^*=\gamma_1[F]$ which behaves in line with traditional theories. Physically $[F]^*$ is the free surfactant concentration based on the accessible volume. Fig. 8(b) shows the predicted size distributions. For [S]=0.12 the agreement is exact since we have extracted all our information at this concentration. The predictions at [S]=0.02 and [S]=0.065 correspond closely to the simulated data, and

therefore support the interpretation in terms of excluded volume.

The standard state chemical potential difference, $(\mu_s^o - \mu_1^o)/kT$, and the excluded volume terms, $\beta_1(r,s)$, are expected to be functions of temperature. Extrapolation from the information obtained at $T_r = 0.60$ to other temperatures requires knowledge of this functional dependence on T and therefore has not been performed. The approach described in this paper, has however, been employed equally successfully at the other temperatures.

IV. CONCLUSION

Stochastic Dynamics simulations have been employed to investigate the self-assembly of model amphiphiles A_2B_2. The effect of temperature and surfactant concentration on the micelle size distribution was obtained. The micelle shape was quantified using the eigenvalues of the moment of inertia matrix and the spherically averaged radial distribution function. A drop in free surfactant concentration observed at high total surfactant concentration was attributed to excluded volume effects and taken into account using a second virial coefficient. In contrast to the approach of Desplat and Care,[12] the dependency of the activity coefficient, γ_s, on aggregate size was also taken into account, and shown to be important for intermediate aggregation numbers. Excellent agreement was obtained between the simulated results and the predictions based on the excluded volume approach over the entire concentration range. We have demonstrated that Stochastic Dynamics simulations provide a computationally efficient means of investigating the self-assembly process of small model amphiphiles. Future work will be directed towards understanding the dynamics of self-assembly and incorporating the effect of solvent structure through a potential of mean force.

ACKNOWLEDGMENTS

This work was supported by the National Science Foundation and NASA.

[1] C. Tanford, *The Hydrophobic Effect* (Wiley, New York, 1980).
[2] P. Mukerjee, J. Phys. Chem. **76**, 565 (1972).
[3] E. Ruckenstein and R. Nagarajan, in *Micellization, Solubilization, and Microemulsions*, edited by K. L. Mittal (Plenum, New York, 1977), Vol. 1, p. 133.
[4] D. Blankschtein, G. Thurston, and G. Benedek, J. Chem. Phys. **85**, 7268 (1986).
[5] R. Nagarajan, Colloid. Surf. A **71**, 39 (1993).
[6] J. Israelachvili, *Intermolecular and Surface Forces* (Academic, London, 1991).
[7] R. G. Larson, J. Chem. Phys. **89**, 1642 (1988).
[8] A. D. Mackie, K. Onur, and A. Z. Panagiotopolous, J. Chem. Phys. **104**, 3718 (1996).
[9] R. G. Larson, J. Chem. Phys. **96**, 7904 (1992).
[10] Y. Wang, W. L. Mattice, and D. H. Napper, Langmuir **9**, 66 (1993).
[11] Y. Wang, W. L. Mattice, and D. H. Napper, Macromolecules **25**, 4073 (1992).
[12] J. -C. Desplat and C. M. Care, Mol. Phys. **87**, 441 (1996).
[13] R. E. Goldstein, J. Chem. Phys. **84**, 3367 (1986).
[14] D. Brown and J. H. R. Clarke, J. Phys. Chem. **92**, 2881 (1988).
[15] J. Böcker, J. Brickmann, and P. Bopp, J. Phys. Chem. **98**, 712 (1994).
[16] J. C. Shelly, M. Sprik, and M. Klein, Langmuir **9**, 916 (1993).
[17] J. R. Gunn and K. A. Dawson, J. Chem. Phys. **91**, 6393 (1989).
[18] D. R. Rector, F. van Swol, and J. R. Henderson, Mol. Phys. **82**, 1009 (1994).
[19] B. Smit, P. A. J. Hilbers, K. Esselink, L. A. M. Rupert, and N. M. van Os, J. Phys. Chem. **95**, 6361 (1991).
[20] B. Smit, K. Esselink, P. A. J. Hilbers, N. M. van Os, L. A. M. Rupert, and I. Szleifer, Langmuir **9**, 9 (1993).
[21] S. Karaborni, K. Esselink, P. A. J. Hilbers, B. Smit, J. Karthauser, N. M. van Os, and R. Zana, Science **266**, 254 (1994).
[22] S. Karaborni, N. M. van Os, K. Esselink, and P. A. J. Hilbers, Langmuir **9**, 1175 (1993).
[23] B. J. Palmer and J. Liu, Langmuir **12**, 746 (1996).
[24] B. J. Palmer and J. Liu, Langmuir **12**, 6015 (1996).
[25] M. P. Allen and D. J. Tildesley, *Computer Simulations of Liquids* (Oxford Science, Oxford, 1992).
[26] W. F. van Gunsteren, H. J. C. Berendsen, and J. A. C. Rullmann, Mol. Phys. **44**, 69 (1981).
[27] J. M. Deutch and I. Oppenheim, J. Chem. Phys. **54**, 3547 (1971).
[28] T. L. Hill, *Statistical Mechanics* (Dover, New York, 1956).
[29] W. F. van Gunsteren and H. J. C. Berendsen, in *NATO Advance Science Institute Series, The Physics of Superionic Conductors and Electrode Materials*, edited by J. W. Perram, (Plenum, New York, 1980), p. 241.
[30] T. Matsuda, G. D. Smith, R. G. Winkler, and D. Y. Yoon, Macromolecules **28**, 165 (1995).
[31] P. E. Smith, B. M. Pettitt, and M. Karplus, J. Phys. Chem. **97**, 6907 (1993).
[32] R. W. Pastor, R. M. Venable, and M. Karplus, J. Chem. Phys. **89**, 1112 (1988).
[33] M. Murat and G. S. Grest, Macromolecules **29**, 1278 (1996).
[34] R. G. Winkler, T. Matsuda, and D. Y. Yoon, J. Chem. Phys. **98**, 729 (1993).
[35] W. F. van Gunsteren and H. J. C. Berendsen, Mol. Phys. **45**, 637 (1982).
[36] W. F. van Gunsteren and H. J. C. Berendsen, Mol. Simul. **1**, 173 (1988).
[37] K. Binder, *Monte Carlo and Molecular Dynamics Simulations in Polymer Science* (Oxford University, New York, 1995).
[38] J. -P. Ryckaert, G. Ciccotti, and H. J. C. Berendsen, J. Comp. Phys. **23**, 327 (1977).
[39] W. F. van Gunsteren and H. J. C. Berendsen, in *NATO Advance Science Institute Series, The Physics of Superionic Conductors and Electrode Materials*, edited by J. W. Perram (Plenum, New York, 1980), p. 221.
[40] R. J. Hunter, *Foundations of Colloid Science* (Oxford Science, Oxford, 1991), Vol. 1.
[41] T. Haliloğu and W. L. Mattice, Chem. Eng. Sci. **49**, 2851 (1994).
[42] P. Adriani, Y. Wang, and W. L. Mattice, J. Chem. Phys. **100**, 7718 (1994).
[43] I. Johnson, G. Olofsson, and B. Jönsson, J. Chem. Soc. Faraday Trans. 1 **83**, 3331 (1987).
[44] M. Kahlweit and M. Teubner, Adv. Colloid Interface Sci. **13**, 1 (1980).
[45] L. Leibler, H. Orland, and J. C. Wheeler, J. Chem. Phys. **79**, 3550 (1983).
[46] L. Onsager, Ann. NY Acad. Sci. **51**, 627 (1949).
[47] A. Ben-Shaul and W. M. Gelbart, J. Phys. Chem. **86**, 316 (1982).
[48] H. Wennerström and B. Lindman, Phys. Rep. **52**, 1 (1979).